A thick-walled sheet moulding compound automotive component: manufacturing and performance

L. M. Martulli[1,2,*,a], Thomas Creemers[2,a], Erich Schöberl[3], Nicholas Hale[3], Martin Kerschbaum[1], Stepan V. Lomov[2], Yentl Swolfs[2]

[1]Toyota Motor Europe, Material Engineering, Hoge Wei 33, 1930 Zaventem, Belgium

[2]Department of Materials Engineering, KU Leuven, Kasteelpark Arenberg 44, B-3001 Leuven, Belgium

[3]Engineering Materials, Faculty of Engineering and Physical Sciences, University of Southampton, Southampton SO17 1BJ, UK

* Corresponding author: luca.martulli@toyota-europe.com

[a] These authors contributed equally to this work.

Abstract

Carbon Fibre Sheet Moulding Compounds (CF-SMCs) are lightweight materials very suitable for automotive parts. So far, their use was limited to thin components. This work presents a feasibility study on the compression moulding of a thick-walled SMC component, with a compound of randomly oriented chopped carbon fibre tapes. Bending tests were used to evaluate the effects of the manufacturing conditions on the mechanical performance. The choice of the charge pattern configuration played the paramount role in the final part performance, especially via the creation of weld surfaces, leading to a maximum strength difference of over 400%. The moulding temperature, pressure and cooling method showed no statistically significant influence on both strength and stiffness of the part. The results of this work can be used as a starting point in the design of manufacturing processes for thick SMC components.

1 Introduction

Carbon reinforced composites have spread very quickly to motorsport and aerospace thanks to their high specific properties. The most classical use of those materials is layered laminates, which makes them suitable for shell-like structures, like aerofoils or outer skins. However, laminated composites tend to be unsuitable for bulkier structural components, like landing gears or car chassis parts. A possible solution to exploit the lightweight capabilities of composites in such components is to use discontinuous composites. Thanks to manufacturing techniques like injection or compression moulding, those materials can be used for thick complex 3D geometries [1]. However, the mechanical properties of injection moulded short fibre composites are too low for structural parts. On the other hand, compression moulded Tow-Based Discontinuous Composites (TBDCs), such as Carbon Fibre Sheet Moulding Compounds (CF-SMC), can serve this purpose.

CF-SMCs are made of chopped carbon fibre tows (or strands) randomly spread in a partially cured thermoset (as in the present paper) or thermoplastic resin. The prepreg sheets that are created in this way are then compression moulded into the final shape. The high aspect ratio of the tows limits the detrimental effects of their discontinuity on the composite performance [2–5], while compression moulding allow short cycle times [6]. As a results, SMCs are an excellent compromise between the good mechanical performance of continuous laminates and the high manufacturability of short fibre composites [2,7,8].

The TBDCs microstructure was investigated using micro Computed X-ray Tomography (µCT) in [9,10] for the case of a no-flow moulding. In this case the tows were mostly

intact, and their orientation was uniformly planar random. On the contrary, high in-mould flow causes high in-plane tow distortion, as well cracks and voids [11]. In all cases, out-of-plane distortion was small, and tows remained mainly planar.

Scientific literature on material characterisation of TBDCs at coupon level is extensive [2,7,11–19]. Their stiffness is usually comparable to that of quasi-isotropic laminates, while their strength and elongation to failure is significantly lower [11,16–18]. In addition, high notch-insensitivity and damage tolerance for these materials has been shown [11,20–22]. All those works focus on characterization of randomly-oriented, low in-mould flow TBDCs.

A much smaller number of works investigates the link between manufacturing and mechanical properties [11,15,23]. However, those works were mainly focused on the induced tow orientation resulting from high in-mould flow, rather than on the effect of moulding parameters. A rare exception are Landry and Hubert [24], who observed surface and internal voids caused by loss of contact with mould walls. This was reproduced by varying both moulding and cooling pressure. Surface defects caused a higher reduction of compressive strength than internal defects. Similarly, Wan and Takahashi [25] found higher tensile and compressive properties of chopped carbon fibre tape reinforced thermoplastics when moulded at higher pressure. This however was due to a better impregnation of the dry tapes. It is therefore questionable whether this conclusion extends to SMC, where the tows are already pre-impregnated with a thermoset matrix.

Some studies also dealt with complex parts made of TBDCs. LeBlanc et al. [26,27] manufactured T-shaped brackets using randomly-oriented thermoplastic strands. Lower

processing temperatures and larger strand sizes required higher pressures to completely

fill the rib. For the same conditions, higher pressure or lower temperature led to lower

porosity levels. Interestingly, this did not result in different mechanical behaviour in

short-beam bending tests of coupons cut from the component. This suggests that

porosity might have limited effects on the bending properties of these materials,

although compressive strength was shown to be affected [24]. Component testing also

showed no mechanical dependence on temperature, pressure and strand sizes. On the

other hand, weld line formation led to a component strength reduction of up to 60%.

Eguemann et al. [28] designed a composite aerospace hinge using different

manufacturing techniques. For this complex shape, SMCs with 20 mm tow lengths

showed comparable strength to that of classical lamination manufacturing. However,

due to the high scatter in strength, a 10 mm UD tow length was judged more suitable.

Their TBDC hinge design led to an 80% weight reduction compared to the steel hinge.

Overall, compression moulded TBDCs parts were 185% stiffer and between 15% and

65% stronger than injection moulded components.

The thickness of these and other compression moulded TBDCs parts reported in

literature [29,30] never exceeded 4 mm. This is due to the intrinsic 2D nature of the

SMC sheets. However, compression moulding allows SMCs to be exploited for thicker

parts [1]. To investigate this opportunity, a 3D component is manufactured and tested in

this work. The nominal wall thickness of the part is 15 mm. Different charge patterns

are first evaluated, to better identify their effect on the mechanical performance. Then,

the moulding temperature, pressure and cooling method will be varied to assess their

effect on mechanical performance. Bending tests will be performed as reference tests

for both the investigations. Micro-Computed Tomography (μCT) before, Digital Image

Correlation (DIC) during and fractography after testing will allow for a better

understanding of the overall material and component response.

2 Materials & methods

2.1 Automotive component and materials

Fig. 1 shows the automotive component object of this study. It is inspired by an actual

chassis part. The nominal cross-section wall thickness is 15 mm, although the effective

thickness can be significantly higher in transition areas. The two steel inserts serve as

load introduction features. Bending is selected as load case, as it is the most

representative of the actual load case of the real component. The nomenclature

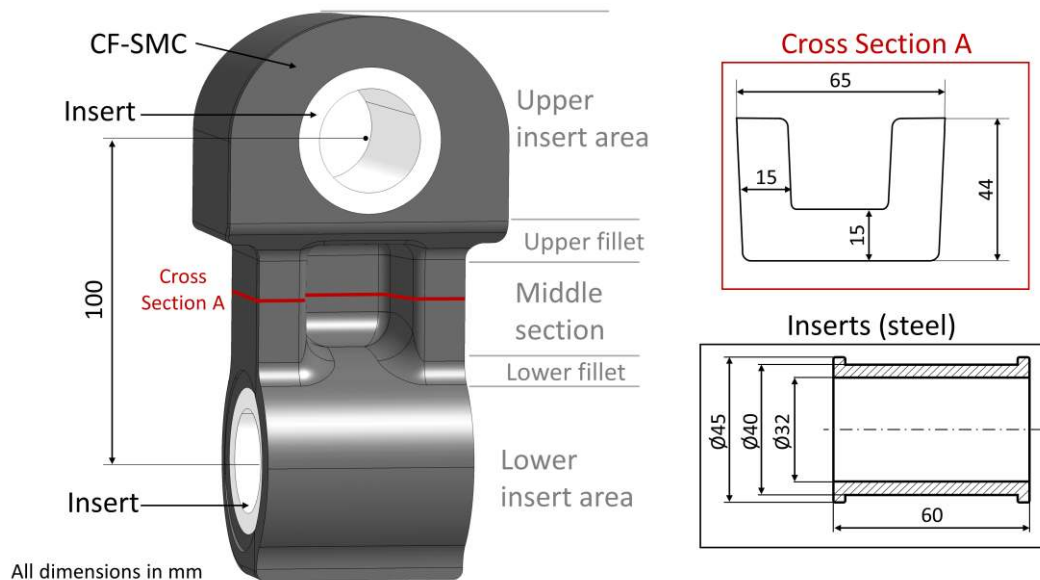introduced in Fig. 1 will be used in the rest of the paper.

Fig. 1: 3D image of the geometry demonstrator, derived from an actual chassis part. Cross-section and inserts dimensions are specified (in mm).

Mitsubishi Chemical Carbon Fiber and Composites GmbH's STR120N [31], a

commercially available SMC, was used as prepreg material for the mouldings. It is

5

made of 42% volume fraction of TR50S [32] carbon fibre chopped strands, randomly dispersed in a B-staged vinyl ester resin. The strand dimensions were 25.4 mm x 8 mm x 0.115 mm with a filament count of 15K. Table 1 shows the properties of the fibres, while Table 2 shows the properties of the cured SMC, both as reported by the supplier. Moreover, mechanical characterisation of the cured SMC was reported in [11,16]. The prepregs were supplied in the form of sheets, that were cut according to the considered Charge Pattern (CP), as discussed in section 2.2.1. The metallic inserts were made of standard construction steel with an approximate yield strength of 200 MPa.

Table 1: Property of the carbon fibres (dry bundle test)

Tensile Strength	Tensile Modulus	Elongation	Fibre diameter
4900 MPa	240 GPa	2.0%	6.8 μm

Table 2: Properties of the cured SMC [31]

Tensile Strength	Tensile Modulus	Bending Strength	Bending Modulus
150 MPa	33 GPa	330 MPa	25 GPa

2.2 Compression moulding

A Fontijne Holland hydraulic press was used for compression moulding. The press was displacement controlled, which has the drawback of not allowing a precise control on the moulding pressure. Its maximum closing force is 1000 kN; the platen dimensions are 700 x 750 mm, distanced at 650 mm at maximum opening. Heating is done with electric resistance heaters. A steel mould was manufactured specifically for this part.

2.2.1 Charge pattern evaluation

In the first part of the study, several parts were compression moulded using different CPs. For all the CPs, the prepreg sheets were cut by hand in the different required shapes, and the target weight was 670 g ± 8 g. All the CPs are shown in Fig. 2 with the subsequent placement steps being:

- CP-A: five plies were wrapped around each insert, and then 20-26 more stacked in the middle.

- CP-B: five plies were wrapped around the left-hand side insert. Five plies were wrapped around the right-hand side insert in a U-shaped fashion. Finally, 15-19 plies were stacked in the middle.

- CP-C: five plies were wrapped around the left-hand side insert in a C-shape with a longer upper edge. Then, 27-29 plies were cut following the net-shape of the mould, and then stacked on the right-hand side of the mould.

- CP-D: five plies were wrapped around the left-hand side insert in a C-shape with a longer upper edge. Then, five plies were wrapped around the right-hand side insert in a U-shaped fashion. 15-19 plies were then stacked in the middle.

For all the CPs described above, the moulding temperature was 140 °C and maximum moulding force was 800 kN ± 200 kN. The parts were cooled in open air.

For the investigations on moulding parameters, a fifth CP was used as a potential improvement of CP-D. Still referring to Fig. 2:

- CP-D': five plies were wrapped in a U-shaped fashion around each insert, instead of only the right-hand side one. 15-19 plies were then stacked in the middle.
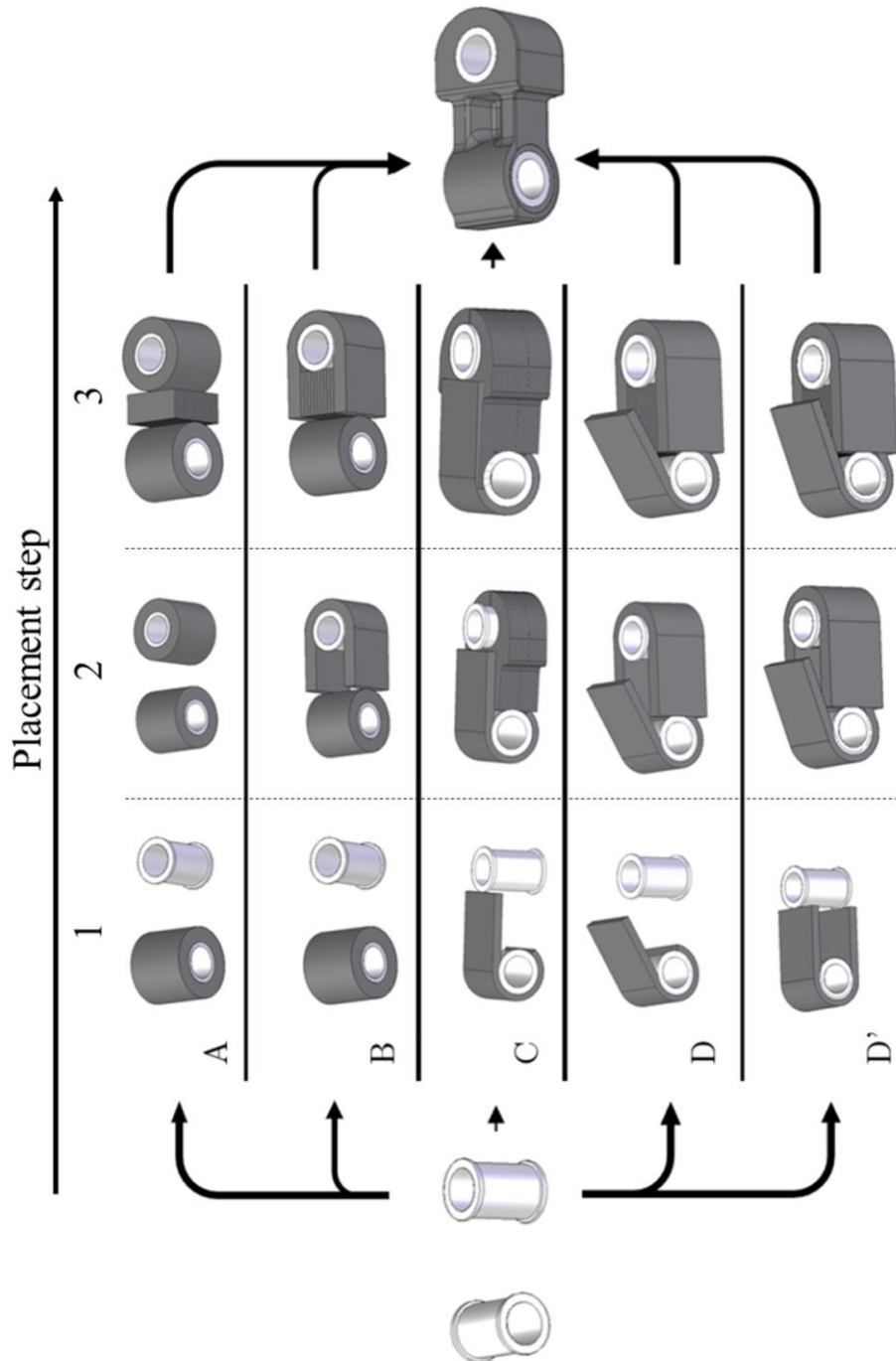

Fig. 2: The different charge patterns, described as subsequent placement steps of the prepregs.

Despite the known detrimental effects of weld lines in injection or compression

moulded plastics, it was practically impossible to produce a weld line-free part. Due to

the 3D geometry, we will consistently use the term 'weld-surface'. To prevent charge

preheating before the closing of the mould, the plies were arranged in three or four

stacks outside of the mould. This allowed the time between the placement of the first

stack in the cavity and the complete closing of the mould to be limited to about fifteen

seconds. The heating of the charge before the mould closure is therefore negligible.

Finally, note that all the plies have the same thickness, and the different number of plies

in the CPs is due to their different shapes and sizes. For example, in CP-B, CP-D and

CP-D', the U-shaped stacks are rectangles of 180x60 mm, while the ones stacked in the

middle are 40x60 mm.

2.2.2 Moulding parameters variation

The parameters of this investigation are reported in Table 3. Despite the press being

displacement-controlled, two significantly different levels of force were achieved by

changing the press settings. The moulding force was constantly monitored during the

manufacturing. Fig. 3 shows the typical curves of the recorded force for each of the

considered modes at both 130°C and 140°C moulding temperature. At first, after a peak

at its maximum value, the applied force decreases by less than 10% in about 300-350 s

and 180 s for the 130°C and 140°C, respectively. Then, due to curing and subsequent

shrinking, a more rapid and intense drop is recorded. The final steady state regime

suggests that the component was fully cured, and thus ready for demoulding. It is

interesting to notice that full curing of this thick-walled component was achieved

between 6 and 7 minutes of moulding at 140°C. This is more than the 2-5 minutes

suggested at the same temperature by the supplier for thin panels [31]. Full curing at

130°C required almost 10 minutes.

Two methods were used to cool the parts, referred to in the rest of the paper as "open

air" and "controlled", respectively. The first method was cooling in open air, whereas

the second one was to place them in an oven at 80°C for 24 hours after demoulding,

followed by cooling in open air. The temperature of 80°C was chosen as the average of

the moulding temperature and room temperatures. The 24 hours were selected to ensure

that the entire part would reach 80°C, before the second stage of cooling.
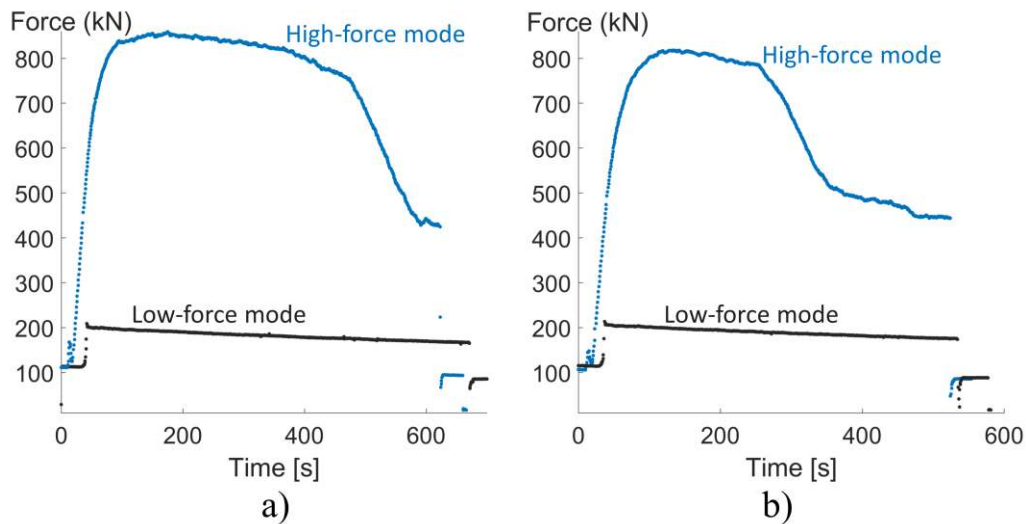
Fig. 3: Moulding force for a) 130°C and b) 140°C moulding.

Following a factorial design approach [33] eight different combinations of the two

levels of temperature – pressure – cooling exist. Two replicates per combination were

moulded, leading to a total of 16 parts. It is to be noticed that, although [33] suggests to

fully randomise the sequence of the experiments, this was not possible for the moulding

temperature. The required cooling and heating of the entire steel mould by 10°C would

have been too time-consuming.

Table 3: Moulding parameters varied for the investigation on their effects on the final mechanical properties.

	Maximum moulding force (F)	Moulding temperature (T)	Cooling method (C)
Level 1	200 kN ± 50 kN	130°C	Open air
Level 2	800 kN ± 200 kN	140°C	Controlled

2.3 Bending tests

The bending test fixture is shown in Fig. 4. All its parts are made of high-resistance stainless steel with a yield strength above 600 MPa.

To install the SMC component in the bending fixture, it is first placed on a steel block, to lift it from the bottom plate of the machine (see Fig. 4a); a plate is placed on one of the sides of the part, and fixed with bolts (see Fig. 4b). Finally, a fork-lug connection introduces load in the other end of the component (see Fig. 4c). The fork is shown in Fig. 4d. High scatter in the bending stiffness was observed in the very first batch of tests. After this observation, the upper bolts were tightened to a consistent torque value of 20 Nm. The scatter was significantly reduced after this operation. The resulting boundary conditions are show in Fig. 5, with a detail of the fork-lug connection in Fig. 5b.
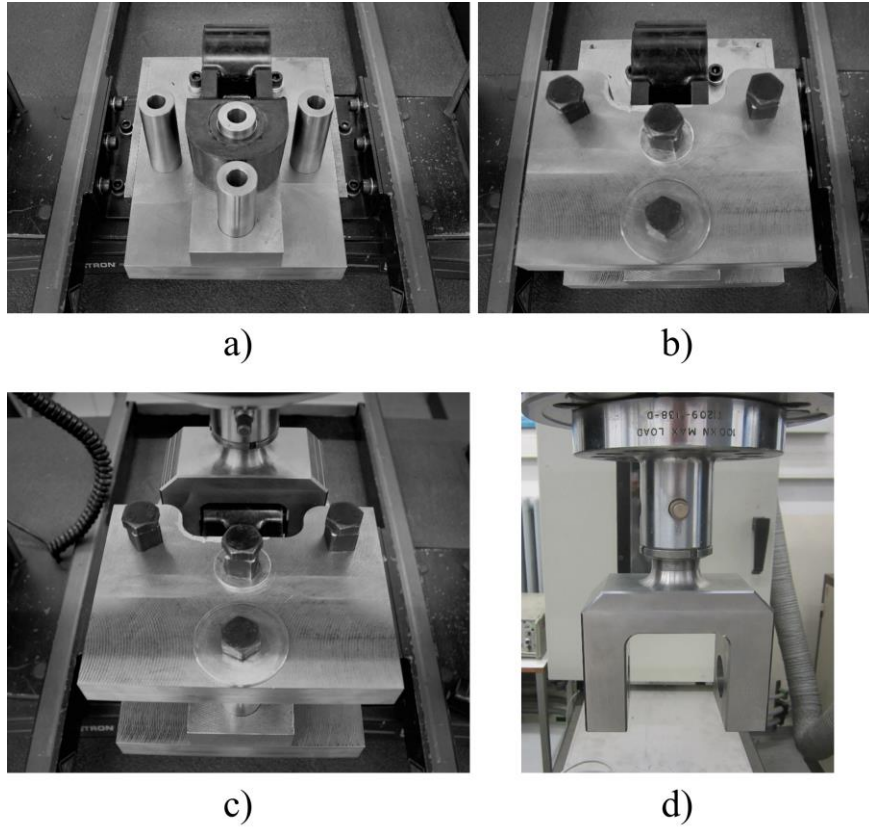
Fig. 4: Experimental set ups: a,b,c) subsequent mounting steps and d) the fork used to introduce the load.
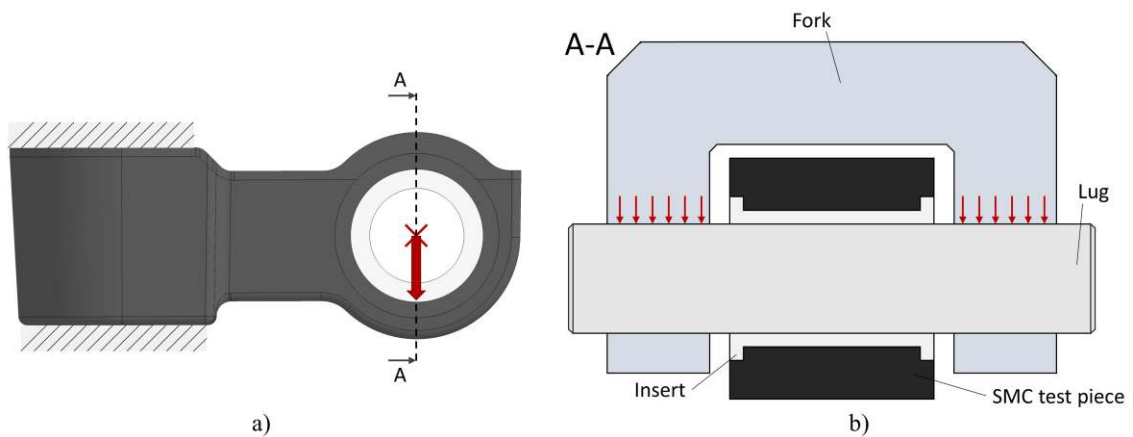

Fig. 5: The bending test of the component: a) boundary conditions of the part in a side view and b) a cross-sectional view of the fork-lug connection.

An Instron 5985 machine was used, with a load cell of 250 kN, and a displacement rate of 2 mm/min. The tests were stopped after a total applied displacement of 10 mm. The machine crosshead displacement was used as the applied displacement.

12

3D DIC was used on some of the parts to monitor the strain map and the eventual crack formation. The parts were sprayed with a white speckle pattern on the surface subjected to tensile stress for this purpose. Two cameras were positioned symmetrically above the fixture, 30° apart from each other. Between them, a diffuse light source was used. VIC-3D was used to extract strain values from the images.

2.4 X ray micro-CT

A X-TEK HMX system was used to scan a CP-B, a CP-D and a CP-D' part, moulded at 140°C and in high-pressure mode, and cooled down in open air. Voltage and current were 160 kV and 137 µA, respectively. Achieved resolution was 53 µm per pixel. Only the middle section and fillets of each part were scanned successfully; the artefacts caused by the metallic inserts prevented the investigation in the other regions.

2.5 Scanning electron microscopy

A XL30 FEG Scanning Electron Microscope (SEM) was used to investigate the fracture surfaces of parts with different CPs. One CP-C component and two components for the other CPs were analysed. The parts were cut to fit them in the SEM; a minimum distance of 10 mm between the cut and fracture surface was maintained, not to alter the failure surface. A 10 nm thick gold-palladium coating was applied prior to the scanning.

3 Results

3.1 Charge Patterns investigation

3.1.1 µCT analysis

Fig. 6 compares the same µCT slices of the CP-B and CP-D' scanned part. No significant difference was found between the CP-D and the CP-D' part.
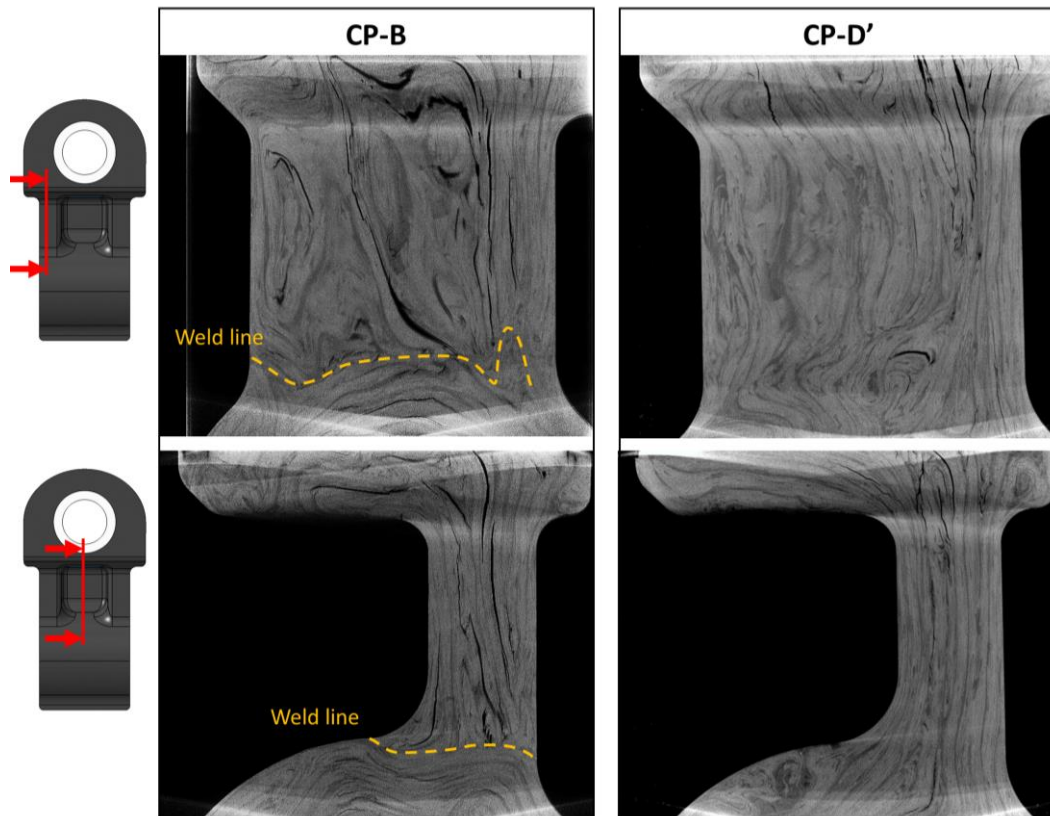
13

Fig. 6: Comparison of µCT slices for a CP-B and a CP-D' component

Firstly, it is worth noting the abundance of cracks in both parts. Those cracks often follow the orientation of the tows, but the low scan resolution prevent to distinguish between delamination and intra-tow failure. Cracks were more commonly observed in correspondence of wrinkled, bent or swirled tows. Matrix rich areas were also often site of cracks, as shown in Fig. 7. All these defects probably originated during cooling: no load was yet applied on those parts, and a tickling noise was heard during the cool down phase. On one hand, the presence of so many defects makes the use of CF-SMC for thick parts difficult. On the other hand, these materials have been reported not to be affected by manufacturing defects, like cracks and voids [11].
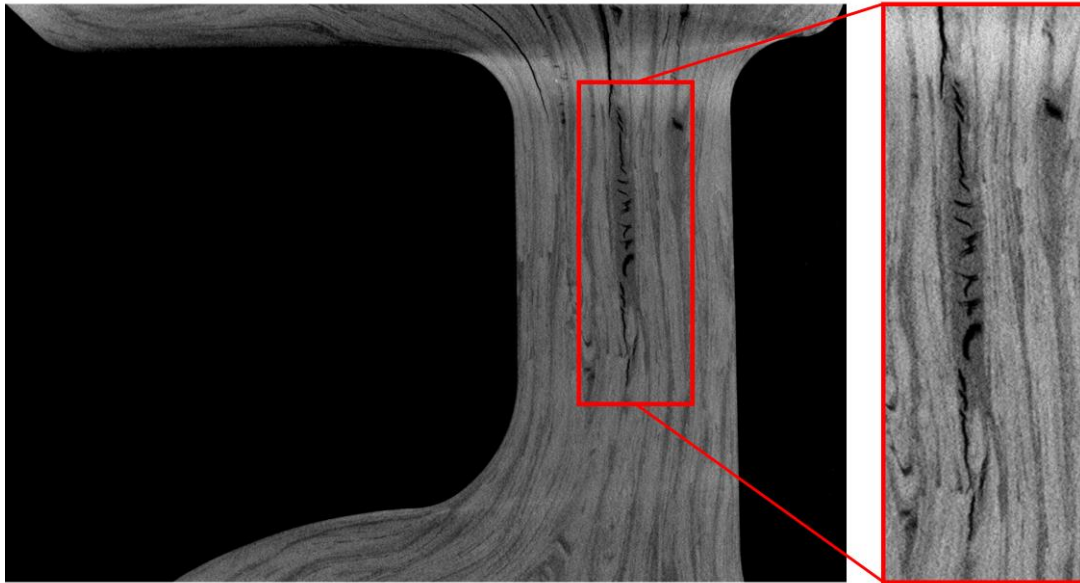
Fig. 7: Slice of a CP-D' part, showing a crack in a resin pocket.

Fig. 6 also shows important difference on the microstructures of the two parts. The weld surface present in the CP-B part abruptly separates distinct regions of different tow orientations. No cracks were observed running through the weld surface. The transition between different areas is much smoother, with tows continuously running throughout the part length. Such smooth transition also reduced the presence of distorted tows, and thus of cracks.

This preliminary investigation already highlights the crucial importance in the correct choice of the charge pattern when dealing with thick SMC components.

3.1.2 Mechanical testing

Table 4 reports the results of the bending tests of the components moulded with different CPs. Bending rigidity and strength are defined in Fig. 8a.

Table 4: Summary of bending tests results ("±" denotes the standard deviation)

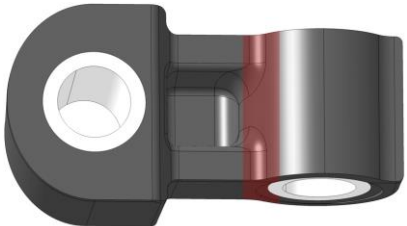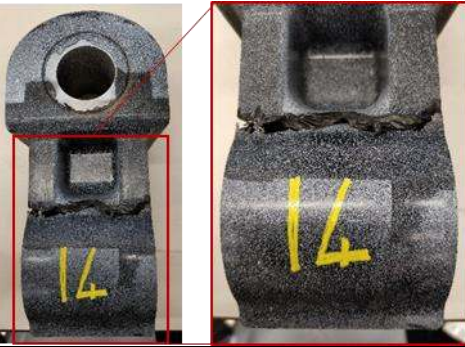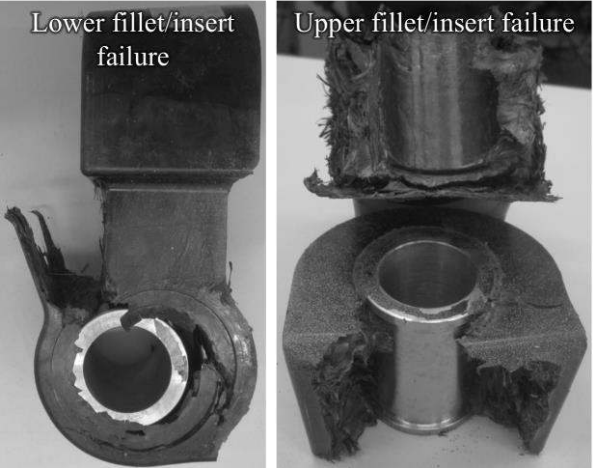| CP	Number of components tested	Rigidity (kN/mm)	Strength (kN)
A	5	7.2 ± 1.3	6.7 ± 3.1
B	10	8.7 ± 1.1	13.4 ± 1.4
C	3	8.7 ± 0.6	18.7 ± 1.5
D	4	9.2 ± 1.2	28.3 ± 8.0
D'	18	8.5 ± 1	22.5 ± 3.0
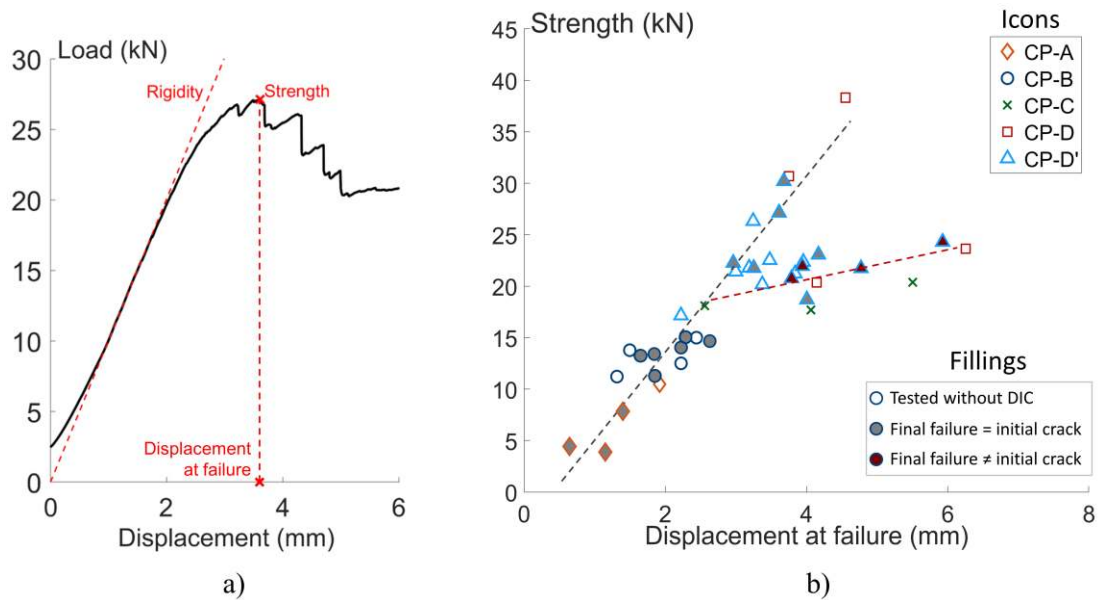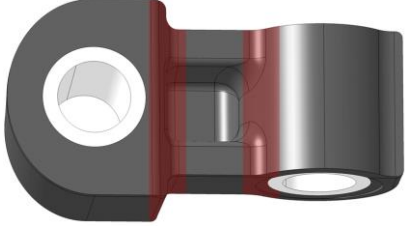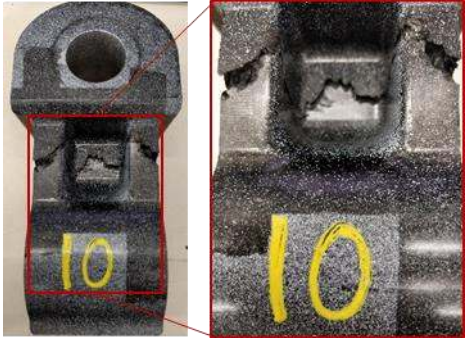
Fig. 8: Bending test results: a) Definition of bending strength, rigidity and displacement at failure and b) failure load against displacement at failure for all components.

Fig. 8b shows the results of the same bending tests, in terms of bending strength and relative displacement. Moreover, locations of the weld surfaces, as expected from the CP configuration (see Fig. 2) and failure location are reported in Table 5.

Table 5: Location of the weld surfaces and ultimate failure

CP	Expected weld surfaces location (in red)	Failure location
A		Varied between both fillets and middle section
B		All in bottom fillet
C D D'	Spread and fragmented	Fourteen parts failed between lower fillet and insert, eleven between upper fillet and insert. Failure often involved insert debonding.

In Fig. 8b, two main trends are recognisable, indicated by the dashed lines. A possible explanation for this lies in the different evolution of the crack leading to failure. With DIC monitoring it is possible to compare the position of the initial visible crack with the final failure location. For most of the components, the failure location corresponded to the location of the first crack (grey filled markers in Fig. 8b). However, a significant portion of them failed elsewhere (red filled markers in Fig. 8b). For those components, the presence of cracks in multiple locations led to an increased compliance and a reduced failure load. This analysis further emphasizes the high variability of the failure behaviour of these materials. Similar unpredictability was also reported in [13] for coupons.

As it is seen in Fig. 8b, CP-A components performed the worst. The presence of two weld surfaces explains not only the low performance, but also the high scatter observed in the strengths, as the weaker spot varied from part to part. As a further confirmation, the CP-A parts failed alternatively in one of the two weld surfaces, or even between them.

Parts moulded with CP-B performed better than CP-A. Those parts had only one weld surface, and all consistently failed in its location, despite the abundance of cracks observed in other locations (see section 3.1.1). Clearly, CF-SMCs are more sensitive to weld surfaces than to cracks and voids originating in manufacturing. Consistency in the failure behaviour is also evident from the low dispersion of the bending strengths, as shown in Table 4. The performance improvement is attributed not only to the removal of one of the weld surfaces, but also in the defect location. In CP-B components, the weld surface is located in a less stressed area, closer to the load introduction and far

from the clamping device. Therefore, compared to CP-A, a higher load is required to reach the failure load.

CP-C, CP-D and CP-D' performed progressively better, but with lower improvements. For all those parts, the weld surface was spread over multiple planes, often perpendicular one to another. This creates a more difficult propagation path for advancing cracks. More energy is indeed required to create a wider crack surface. In addition, some of the planes of the weld surfaces were parallel to the main load direction, and thus loaded in the less detrimental mode II. Indeed, for those CPs, there were no cross-sections entirely made of weld surface. This can be also expressed by stating that, unlike CP-A and CP-B, the other CPs did not have any weld cross-section.

The different performance in the components is thus attributed almost entirely to the presence, location and quality of the weld surfaces. Reducing the angle between their plane and the load direction, and spreading and breaking the weld surfaces in multiple planes helped to mitigate their effects. The maximum difference in strength between CP-A and CP-D was of 422%.

The CF-SMC variability can overcome the presence of macro-notches [20–22], micro-structural defects [11] but not the presence of severe weld surfaces. This conclusion is supported by Fig. 9, that shows the principal strain map, obtained via 3D DIC, of a CP-A, CP-B and CP-D' component. The maps are taken at the 97%, 73% and 87% of the failure load, respectively. The strain map of the CP-A and CP-B components are characterised by a single high strain region in correspondence of the failure location. For the CP-D' part, instead, the weld surfaces are not detrimental enough to overcome

19

the material variability, and a much more heterogeneous strain map is observed. This is

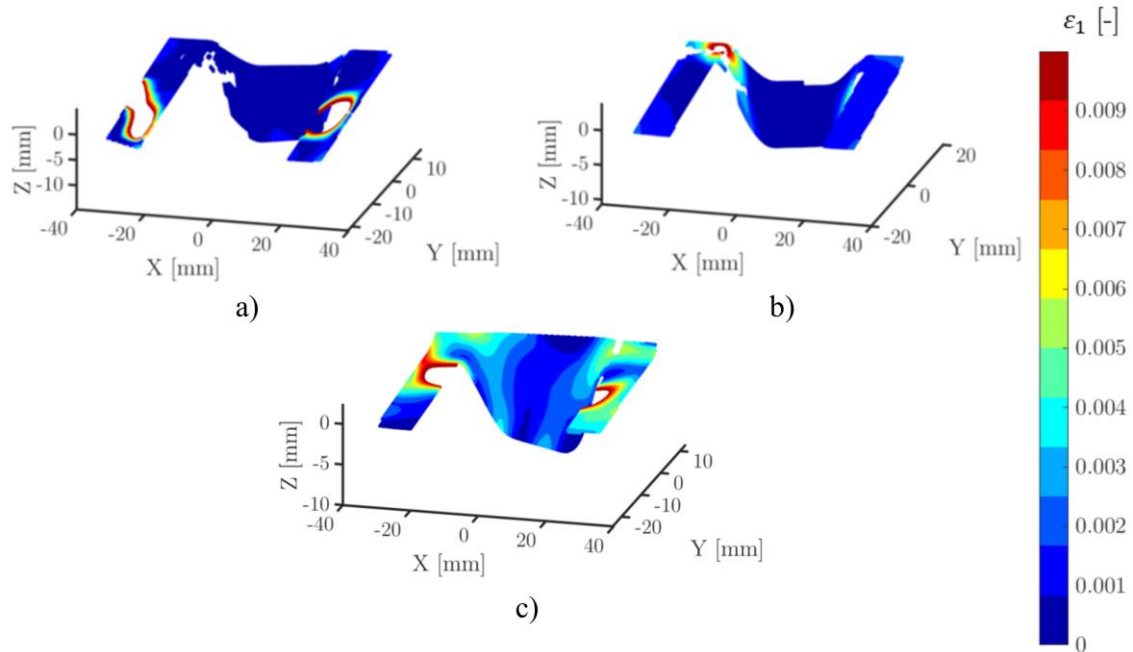much closer to what is commonly observed for TBDCs coupons [2,7,11–13].

Fig. 9: DIC observation before failure for a a) CP-A, b) CP-B and c) CP-D' component.

3.1.3 Failure behaviour

In the following, "intra-tow failure" will indicate longitudinal matrix failure or

debonding within a tow (see Fig. 10a); "trans-tow failure" will indicate a local

translaminar tensile failure of the tow, involving both matrix and fibre failure (see Fig.

10b); "intra-tow failure" will indicate failure happening between adjacent tows as the

result of tow debonding (see Fig. 10c) or matrix cracking (see Fig. 10d). This

nomenclature is derived from laminated composites, replacing intralaminar,
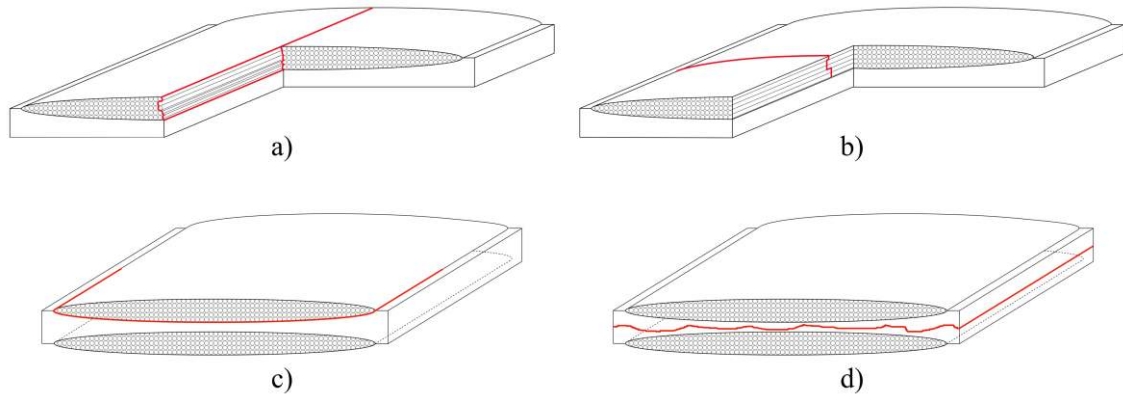
translaminar and interlaminar failures.

Fig. 10: Different failure modes of TBDCs: a) intra-tow failure, b) trans-tow failure and two possible inter-tow failure, c) tow debonding and d) cracking of the inter-tow matrix layer.

The failure surface of a CP-A and a CP-B components was investigated with a SEM Only on the first 30 mm from the outer surface were observed, as it was the area failed in tensile load. A smooth fracture surface with many tows parallel to it, as reported in Fig. 11a and Fig. 11b, suggests a prevailing inter-tow failure mode. This is a further confirmation of a weld-surface dominated failure. Indeed, these defects prevent tows from intermingling and entangling with each other, thus creating a favourable crack path among the tows. In Fig. 11a fibre and tow breakage, trans-tow features, are also visible, while scarps and cusps, intra-tow features, are shown in Fig. 11c. These other failure modes were more common in the outer region of the fracture surfaces, that were the most stressed in tension. Inter-tow failure remained however the prevailing mode, as greater magnified SEM micrographs also confirmed: an example is shown in Fig. 11, where imprints of adjacent tows, typically inter-tow feature, are shown.
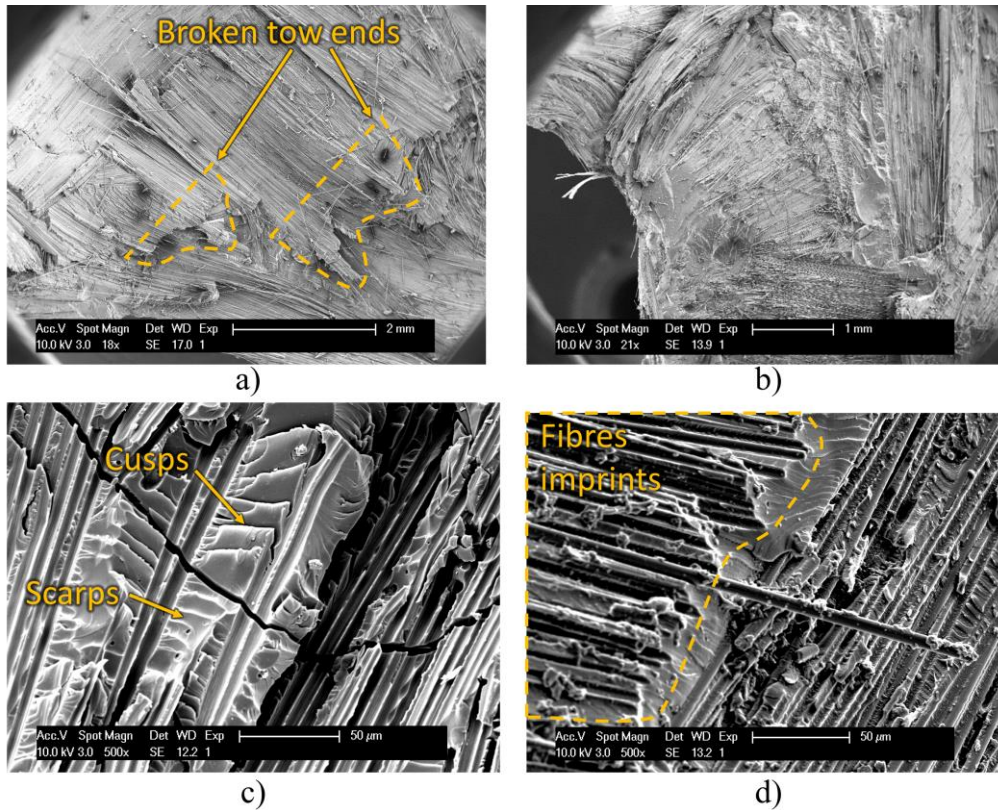
Fig. 11: SEM pictures from of a CP-A and a CP-B component: a) and b) shows inter-tow failure surface, sometimes with broken tow ends; upon magnification, c) intra-tow and d) inter-tow features are visible.

CP-C, CP-D and CP-D' parts showed similar failure behaviour, and will thus be discussed as a single group.

Fig. 12 shows a picture of the failure section of a CP-D' part failed between lower fillet and the lower insert area. Two main failure surfaces can be distinguished. Strands lying in the fracture surface produced a smooth surface, indicating an inter-tow failure type (circled in red in Fig. 12). SEM micrographs of those areas, shown in Fig. 13a and Fig. 13b, show fibre imprints and cusps and scarps. The analysis overall confirmed the prevailing inter-tow nature of the failure, with presence of intra-tow failure as well. The second type of surface (circled in blue in Fig. 12) was observed in correspondence of strands perpendicular to the fracture surface. Those tows were pulled-out, split and broken, as a result of a trans-tow failure, as confirmed by SEM in Fig. 13c. Moreover,

the fracture surface passes through the interface between the insert and the part. This suggests a poor adhesion between the materials. Resin rich areas also affected the crack path, as shown in Fig. 13d. These might sections of the broken weld surfaces, but more investigation is required to confirm such an hypothesis.
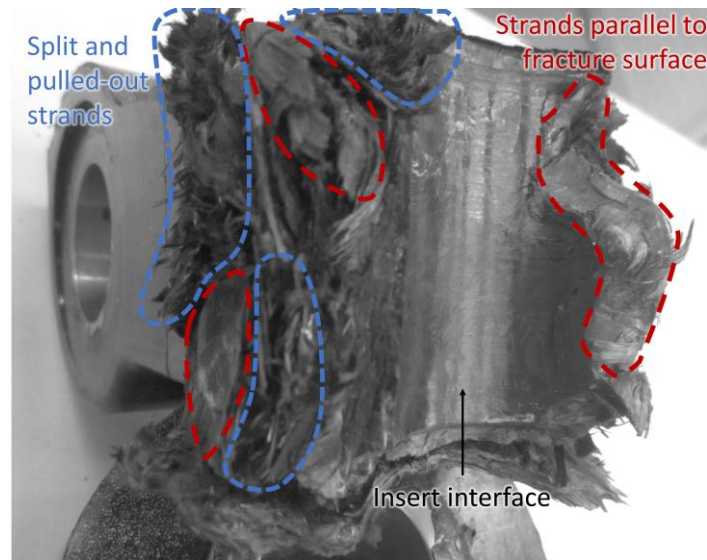

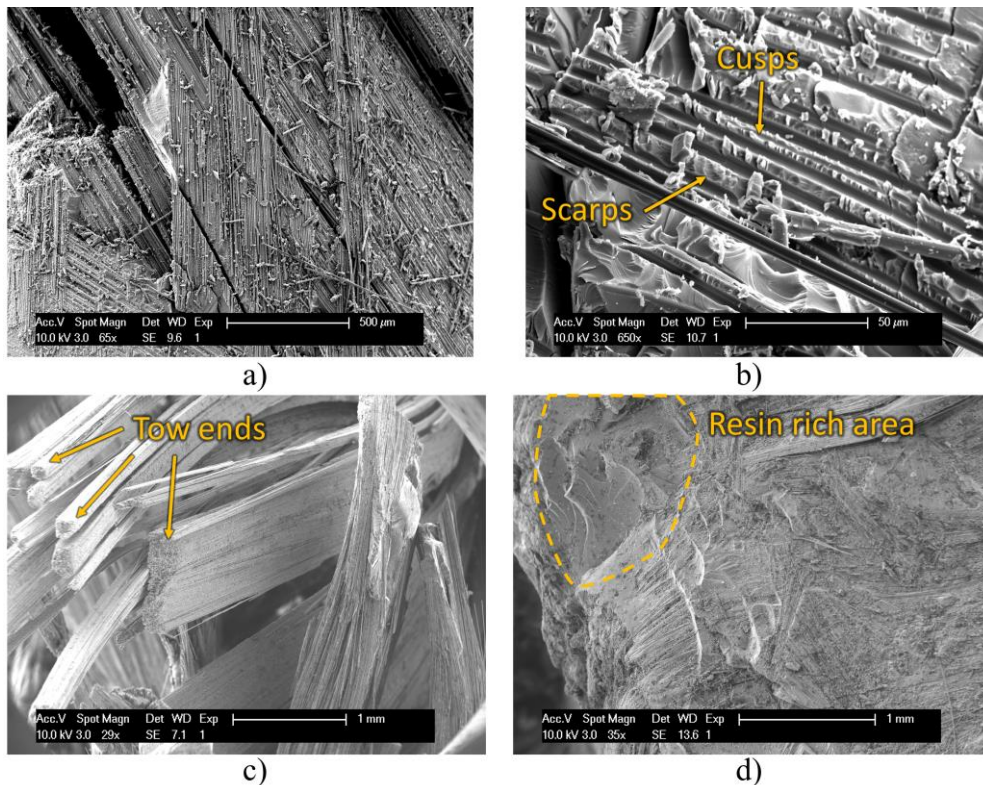**Fig. 12:** Picture of the failure section of a CP-D' component.

Fig. 13: SEM observations of a CP-D' part: a) inter-tow features, b) cusps and scarps originated from intra-tow failure, c) split tow ends and d) resin rich area.

The statistics of the CP-D components was affected by an outlier with a failure load of 38.3 kN (see Fig. 8b). Its failure surface is compared in Fig. 14 to the one of another CP-D part failed at 23.6 kN. As shown in Fig. 14a, the outlier was characterised by a layered microstructure, with little distorted tows mostly parallel to the external boundaries. This is not true for the other CP-D component (see Fig. 14b), which shows heavily distorted tows. Cracks following the wrinkles and swirls were already reported in section 3.1.1, and confirm that these distortions affected the failure of the part.

The high tow distortion is likely caused by the prepreg sheets in the ribs of CP-D components, which are placed perpendicularly to the closing plate of the press (see Fig. 2). When the mould closes, those sheets are then crushed, as shown in Fig. 14.b. This is what most likely happened for every CP-D and CP-D' part, except for the outlier, probably due to random variations in the charge pattern and initial local strand orientations. Therefore, the choice of the charge pattern also affects the creation of additional weaker spots like wrinkled tows. Charge pattern design and consistency is thus a critical point in the manufacturing of performant thick CF-SMC components.
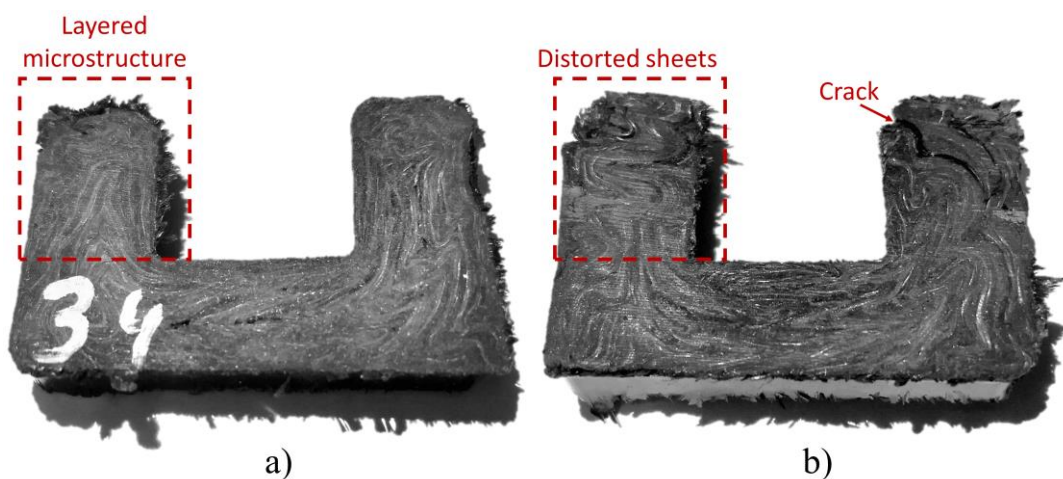

Fig. 14: Failed cross-sections of a) the CP-D outlier, failed at 38.3 kN and of b) another CP-D component, failed at 23.6 kN.

3.2 Moulding parameters investigation

The CP-D' components were moulded with varying moulding temperature, force and cooling method (see Table 3). Fig. 15.a shows the normal probability plot of the maximum load for those parts. As shown, a normal distribution approximates well the data, suggesting that the tested parts all belong to the same population.

This is confirmed by the results of the full factorial design of experiments. Following the indications of [33], the different moulding combinations are named with the capital letter of the parameter of Table 3 set at the level 2. For example, X represents the components moulded at high temperature, low force and cooled in open air, while YZ indicates low temperature, high force and controlled cooling. The combination of low temperature, low pressure and open air does not have a name, as it is the reference against which the statistical significance of the other cases is evaluated. Using a statistical significance level α of 0.05 and a two-tailed Student's t distribution, a threshold value of 2.306 was obtained. As shown by the Pareto chart in Fig. 15b, none of the combination produced a statistically significant variation against the reference.
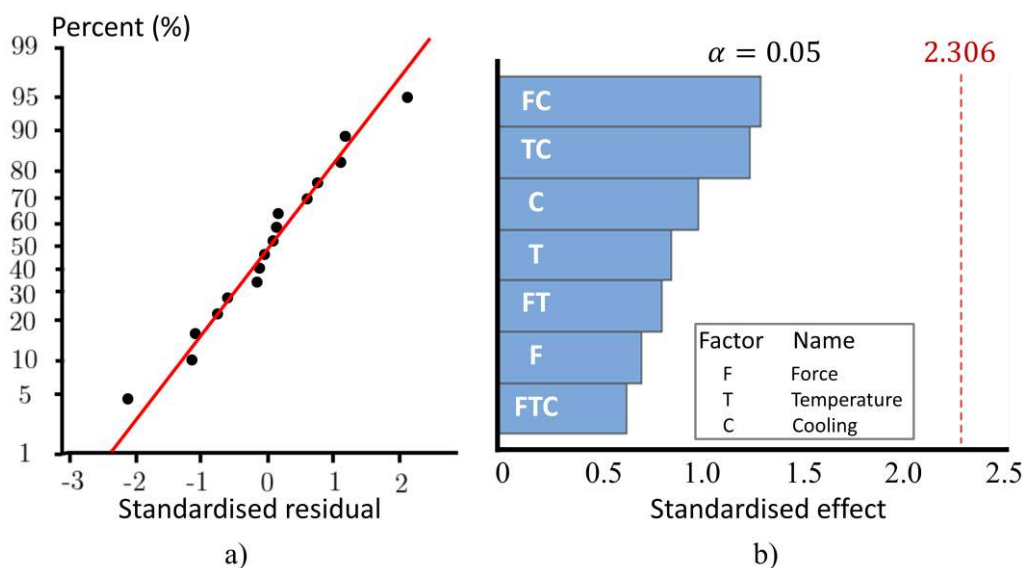

Fig. 15: Statistical analysis of the moulding parameters investigation: a) normal plot of the standardised residuals of the maximum loads and b) Pareto chart of the standardised effects and significance threshold.

This implies that, when dealing with thick 3D SMC parts used for this investigation, the moulding temperature, pressure and cooling method do not significantly affect their bending performance. A possible reason for this result lies in the intrinsic material variability of the material, behind which the effects of those parameters are hidden. . More investigation is needed to understand if the high thickness amplifies or reduces the effect of this variability. On the one hand, a higher thickness might give to the flow more space to distort the tows or orient them in the out-of-plane direction. On the other hand, the presence of more material might hide the effects of such defects. No definitive answer can be thus given at this stage.

4   Conclusions

This study has investigated the feasibility of the compression moulding of a thick CF-SMC component.

Varying the charge pattern during manufacturing led to a difference of 422% in the bending strength of the component. The charge pattern was thus the most influencing parameter, mainly due to two mechanisms. First, carefully varying the charge pattern allowed a reduction of the effects of the weld surfaces. This was achieved by decreasing their number, moving their location from high-stress to low-stress areas and by fragmenting and breaking them in multiple planes. Weld surfaces were observed to be primary defects, always leading to failure a notch-insensitive material like SMC. Indeed, weld surfaces lead to failure even parts with many cracks in other areas. Moreover, varying the charge pattern can vary the amount wrinkles and swirls in the tows. Those have been reported, here and in the literature, to act as potential failure site, and thus minimising those defects is key.

No significant effects were observed when varying the moulding temperature, pressure and cooling rate of the components. This is explained by the fact that the effects of those parameters are likely hidden by the high intrinsic variability of those materials. Interestingly, this SMC variability is reported to also overcome the effects of macro-notches and micro-defects, but was not enough to overcome the effects of the weld lines.

Upon bending, it was also possible to identify the failure mechanisms leading to failure of the part. The failure initiation involves all the three main mechanisms: tow splitting and failure of the tows aligned with the load direction (trans-tow failure) and matrix-cracking and fibre debonding both within a tow (intra-tow failure) and between adjacent tows (inter-tow failure). The propagation of the static crack continues mainly as an inter-tow phenomenon.

The results shown in this work can be used in the preliminary design of manufacturing processes for thick SMC components.

5 Acknowledgments

6 References

[1]   Han CD. Rheology and Processing of Polymeric Materials, Volume 1: Polymer
        Rheology. 2007. https://doi.org/10.1017/CBO9781107415324.004.

[2]   Visweswaraiah SB, Selezneva M, Lessard L, Hubert P. Mechanical
        characterisation and modelling of randomly oriented strand architecture and their
        hybrids – A general review. J Reinf Plast Compos 2018;37:548–80.
        https://doi.org/10.1177/0731684418754360.

[3]   Tucker CL, Liang E. Stiffness predictions for unidirectional short-fiber
        composites: Review and evaluation. Compos Sci Technol 1999;59:655–71.
        https://doi.org/10.1016/S0266-3538(98)00120-1.

[4]   Wan Y, Takahashi J. Tensile properties and aspect ratio simulation of
        transversely isotropic discontinuous carbon fiber reinforced thermoplastics.
        Compos Sci Technol 2016;137:167–76.
        https://doi.org/10.1016/j.compscitech.2016.10.024.

[5]   Kelly A, Tyson WR. Tensile Fibre-Reinforced Metals : Copper/Tungsten and
        Copper/Molybsenum. J Mech Phys Solids 1965;13:329–50.

[6]   Barbero EJ. Introduction to Composite Materials Design. 2nd ed. Taylor &
        Francis Group; 2011.

[7]   Selezneva M, Lessard L. Characterization of mechanical properties of randomly
        oriented strand thermoplastic composites. J Compos Mater 2016;50:2833–51.
        https://doi.org/10.1177/0021998315613129.

[8]   Chang IY, Pratte JF. LDF^{TM} Thermoplastic Composites Technology. J
        Thermoplast Compos Mater 1991;4:227–52.

[9]   Wan Y, Straumit I, Takahashi J, Lomov S V. Micro-CT analysis of internal
        geometry of chopped carbon fiber tapes reinforced thermoplastics. Compos Part
        A Appl Sci Manuf 2016;91:211–21.
        https://doi.org/10.1016/j.compositesa.2016.10.013.

[10]   Wan Y, Straumit I, Takahashi J, Lomov S V. Micro-CT analysis of the
        orientation unevenness in randomly chopped strand composites in relation to the
        strand length. Compos Struct 2018;206:865–75.

https://doi.org/10.1016/j.compstruct.2018.09.002.

[11]   Martulli LM, Muyshondt L, Kerschbaum M, Pimenta S, Lomov S V, Swolfs Y.
        Carbon fibre sheet moulding compounds with high in-mould flow: Linking
        morphology to tensile and compressive properties. Compos Part A Appl Sci
        Manuf 2019;126:105600. https://doi.org/10.1016/j.compositesa.2019.105600.

[12]   Feraboli P, Peitso E, Deleo F, Cleveland T. Characterization of Prepreg-Based
        Discontinuous Carbon Fiber / Epoxy Systems. J Reinf Plast Compos 2009;28.
        https://doi.org/10.1177/0731684408088883.

[13]   Feraboli P, Cleveland T, Ciccu M, Stickler PB, DeOto L. Defect and damage
        analysis of advanced discontinuous carbon/epoxy composite materials. Compos
        Part A Appl Sci Manuf 2010;41:888–901.
        https://doi.org/10.1016/j.compositesa.2010.03.002.

[14]   Feraboli P, Peitso E, Cleveland T, Stickler PB. Modulus Measurement for
        Prepreg-based Discontinuous Carbon Fiber/Epoxy Systems. J Compos Mater
        2009;43:1947–65. https://doi.org/10.1177/0021998309343028.

[15]   Evans AD, Qian CC, Turner TA, Harper LT, Warrior NA. Flow characteristics of
        carbon fibre moulding compounds. Compos Part A Appl Sci Manuf 2016;90:1–
        12. https://doi.org/10.1016/j.compositesa.2016.06.020.

[16]   Nicoletto G, Riva E, Stocchi A. Mechanical Characterization of Advanced
        Random Discontinuous Carbon/Epoxy Composites. Mater Today Proc
        2016;3:1079–84. https://doi.org/10.1016/j.matpr.2016.03.052.

[17]   Denos BR, Kravchenko SGS, Pipes RB. Progressive Failure Analysis in Platelet
        Based Composites Using CT-Measured Local Microstructure. Int. SAMPE Tech.
        Conf., Seattle (WA): 2017. https://doi.org/10.1137/S0036141003433437.

[18]   Piry M, Michaeli W. Stiffness and failure analysis of SMC components
        considering the anisotropic material properties. Macromol Mater Eng 2000;284–
        285:40–5. https://doi.org/· 10.1002/1439-2054(20001201)284:13.3.CO;2-V.

[19]   Johanson K, Harper LT, Johnson MS, Warrior NA. Heterogeneity of
        discontinuous carbon fibre composites: Damage initiation captured by Digital
        Image Correlation. Compos Part A Appl Sci Manuf 2015;68:304–12.
        https://doi.org/10.1016/j.compositesa.2014.10.014.

[20]   Feraboli P, Peitso E, Cleveland T, Stickler PB, Halpin JC. Notched behavior of
        prepreg-based discontinuous carbon fiber/epoxy systems. Compos Part A Appl
        Sci Manuf 2009;40:289–99. https://doi.org/10.1016/j.compositesa.2008.12.012.

[21]   Qian C, Harper L, Turner TA, Warrior NA. Notched behaviour of discontinuous
        carbon fibre composites: Comparison with quasi-isotropic non-crimp fabric.
        Compos Part A Appl Sci Manuf 2011;42:293–302.
        https://doi.org/10.1016/j.compositesa.2010.12.001.

[22] Pimenta S, Ahuja A, Lau AY. Damage Tolerant Tow-Based Discontinuous Composites. 20th Int. Conf. Compos. Mater., Copenhagen, Denmark: n.d.

[23] Nony-Davadie C, Peltier L, Chemisky Y, Surowiec B, Meraghni F. Mechanical characterization of anisotropy on a carbon fiber sheet molding compound composite under quasi-static and fatigue loading. J Compos Mater 2018. https://doi.org/10.1177/0021998318804612.

[24] Landry B, Hubert P. Experimental study of defect formation during processing of randomly-oriented strand carbon/PEEK composites. Compos Part A Appl Sci Manuf 2015;77:301–9. https://doi.org/10.1016/j.compositesa.2015.05.020.

[25] Wan Y, Takahashi J. Tensile and compressive properties of chopped carbon fiber tapes reinforced thermoplastics with different fiber lengths and molding pressures. Compos Part A Appl Sci Manuf 2016;87:271–81. https://doi.org/10.1016/j.compositesa.2016.05.005.

[26] LeBlanc D, Landry B, Levy A, Hubert P, Roy S, Yousefpour A, et al. Study of Processing Conditions on the Forming of Ribbed Features Using Randomly Oriented Strands Thermoplastic Composites. J Am Helicopter Soc 2015;60:1–9. https://doi.org/10.4050/jahs.60.011005.

[27] LeBlanc D, Landry B, Levy A. Compression moulding of complex parts using randomly-oriented strands thermoplastic composites 2014.

[28] Eguemann N, Giger L, Roux M, Dransfeld C, Thiebaud F, Perreux D. Compression moulding of complex parts for the aerospace with discontinuous novel and recycled thermoplastic composite materials. 19th Int Conf Compos Mater 2013:1–11.

[29] Favaloro AJ, Sommer DE, Denos BR, Pipes RB. Simulation of prepreg platelet compression molding: Method and orientation validation. J Rheol (N Y N Y) 2018;62:1443–55. https://doi.org/10.1122/1.5044533.

[30] Denos BR, Sommer DE, Favaloro AJ, Pipes RB, Avery WB. Fiber orientation measurement from mesoscale CT scans of prepreg platelet molded composites. Compos Part A Appl Sci Manuf 2018;114:241–9. https://doi.org/10.1016/j.compositesa.2018.08.024.

[31] Mitsubishi Chemical Corporation. Pyrofil STR120 datasheet n.d.

[32] Mitsubishi Chemical Corporation. TR50s Datasheet n.d.

[33] Montgomery DC, Runger GC. Applied Statistics and Probability for Engineers, 3rd ed. 2003. https://doi.org/10.2307/1269738.